

CLOSING THE SAFETY GAP: SURGICAL CONCEPT ERA-SURE IN VISUAL AUTOREGRESSIVE MODELS

000
001
002
003
004
005 **Anonymous authors**
006 Paper under double-blind review
007
008
009
010

ABSTRACT

011 The rapid progress of visual autoregressive (VAR) models has brought new oppor-
012 tunities for text-to-image generation, but also heightened safety concerns. Existing
013 concept erasure techniques, primarily designed for diffusion models, fail to gener-
014 alize to VARs due to their next-scale token prediction paradigm. In this paper, we
015 first propose a novel VAR Erasure framework **VARE** that enables stable concept
016 erasure in VAR models by leveraging auxiliary visual tokens to reduce fine-tuning
017 intensity. Building upon this, we introduce **S-VARE**, a novel and effective concept
018 erasure method designed for VAR, which incorporates a filtered cross entropy loss
019 to precisely identify and minimally adjust unsafe visual tokens, along with a preser-
020 vation loss to maintain semantic fidelity, addressing the issues such as language
021 drift and reduced diversity introduce by naïve fine-tuning. Extensive experiments
022 demonstrate that our approach achieves surgical concept erasure while preserving
023 generation quality, thereby closing the safety gap in autoregressive text-to-image
024 generation by earlier methods.
025

1 INTRODUCTION

026 The rapid progress of text-to-image generative models (Rombach et al., 2022; Ramesh et al., 2022;
027 Labs, 2024; Han et al., 2025) has significantly enhanced their ability to produce high-quality outputs
028 with strong adherence to text prompt. These advancements are driven not only by improvements
029 in model architectures but also by the availability of large-scale training data (Schuhmann et al.,
030 2022; Byeon et al., 2022). More recently, a new family of generative models known as visual
031 autoregressive models (VAR) (Tian et al., 2024; Han et al., 2025) has been introduced. Unlike
032 traditional autoregressive models that generate visual tokens in a raster-scan order (Chen et al., 2025),
033 VAR models predict visual tokens at progressively larger scale. This hierarchical generation paradigm
034 brings substantial improvements in both image quality and generation speed. Notably, Infinity (Han
035 et al., 2025) has showcased the strong performance of VAR models on high-resolution text-to-image
036 generation tasks. Despite their advantages, current text-to-image VAR models lack effective safety
037 mechanisms and remain susceptible to generating sensitive or inappropriate images. However, such
038 models are often capable of generating unsafe content in response to inappropriate prompts, such
039 as NSFW (Not-Safe-For-Work) images involving pornography and violence (Jiang et al., 2023), or
040 material that may raise copyright concerns (Qu et al., 2023). A more pressing challenge emerges
041 when new undesirable concepts are identified after model training. Reconstructing the training dataset
042 and retraining the model from scratch for each such case imposes an impractical computational
043 burden. This significantly hinders the safe and scalable deployment of text-to-image generation
044 systems in real-world applications.
045

046 Concept Erasure (CE), a family of emerging methods serves as a promising solution for efficiently
047 removing undesirable concepts from generative models. These approaches achieve concept erasure by
048 modifying model components (e.g., cross-attention modules) or Low-Rank Adaptation (LoRA) (Hu
049 et al., 2022) through fine-tuning (Gandikota et al., 2023; Zhang et al., 2024a; Kumari et al., 2023),
050 closed-form solutions (Gandikota et al., 2024), or neuron pruning (Chavhan et al., 2024). Existing
051 methods have been well-studied in the domain of diffusion models (Rombach et al., 2022) based on
052 U-Net (Ronneberger et al., 2015) architectures and follow-up works (Zhang et al., 2025; Gao et al.,
053 2025) have also extended these techniques to FLUX (Labs, 2024), a transformer-based (Vaswani
et al., 2017) diffusion model that employs flow matching (Lipman et al., 2022), demonstrating some
degree of success. However, existing methods developed for diffusion models cannot be directly

054 applied to VAR models, due to the different use of visual GPT-based (Hurst et al., 2024) transformer
 055 and the fact that the prediction targets are visual tokens instead of noise. This results in a clear
 056 methodological gap in concept erasure for this emerging family of generative models.
 057

058 In this work, we examine the limitations of existing CE methods originally developed for diffusion
 059 models when applied to VAR framework. Current approaches align visual tokens independently
 060 at each scale using differential prompts, a procedure reminiscent of aligning diffusion outputs at
 061 individual timesteps. However, this independent alignment introduces cumulative errors across scales,
 062 often leading to severe degradation in image quality. To address this challenge, we first introduce
 063 **VARErasure**, a framework that leverages auxiliary target tokens as additional inputs to mitigate
 064 discrepancies caused by token misalignment. Building on this framework, we further propose **S-
 065 VAR**, a method for surgical concept erasure in VAR models. Unlike prior work that formulates
 066 erasure as a regression problem by minimizing mean squared error (MSE) between predicted and
 067 reference noise in U-Nets, recent advances such as the Infinity model have demonstrated that binary
 068 spherical quantization (BSQ) (Zhao et al., 2024) can improve codebook efficiency by projecting
 069 predictions into a probability space. Inspired by this, we design a filtered cross-entropy loss \mathcal{L}_{FCE}
 070 that measures semantic differences more precisely by computing bit-wise discrepancies between
 071 predicted tokens and quantized targets. Finally, to counter common side effects of naïve fine-tuning,
 072 such as language drift and reduced output diversity, we introduce a preservation loss \mathcal{L}_{Pre} tailored
 073 for VARs, which aligns outputs of the pre-trained and fine-tuned models, safeguarding unrelated
 074 concepts and maintaining generative diversity.
 075

076 In summary, we make the following contributions:
 077

- 078 • We are the first to systematically analysis the challenge of directly applying existing diffusion-
 079 based CE methods to VAR models, and we propose a novel fundamental **VAR** framework
 080 to address this limitation.
- 081 • By analyzing the characteristics of the VAR framework, we identify the limitations of
 082 existing erasure functions and introduce a new concept erasure method **VAR**, which
 083 consists of a filtered erasure loss \mathcal{L}_{FCE} and a preservation loss \mathcal{L}_{Pre} .
- 084 • Extensive experimental results demonstrate that our method successfully erases 97% of
 085 sensitive concepts while causing less than 2% degradation in CLIP score, filling a critical
 086 gap in the safe and efficient deployment of text-to-image generation models.

087 2 RELATED WORKS

088 2.1 VISUAL AUTOREGRESSIVE MODELS

089 To unify visual generation and understanding within a single framework, autoregressive visual
 090 generation models typically first apply vector quantization (VQ) to convert image patches into
 091 discrete visual tokens (Van Den Oord et al., 2017). These models then predict the next visual token in
 092 a determined raster scan order conditioned on previously generated tokens (Yu et al., 2024; Fan et al.,
 093 2024). Building on this pipeline, numerous works (Chen et al., 2025; Deng et al., 2025; Wang et al.,
 094 2024a;b) have developed increasingly powerful architectures for image and video generation tasks.
 095 Recently, Visual Autoregressive Models (VAR) (Tian et al., 2024) introduced a novel next-scale
 096 prediction paradigm that significantly improves generation quality. Subsequent works (Li et al.,
 097 2024; Yao et al., 2024; Zhang et al., 2024b) have explored controllable generation within the VAR
 098 framework, and Infinity (Han et al., 2025) further advances this line of work by employing bit-wise
 099 quantization to enhance scalability and achieves high-quality text-to-image generation with strong
 100 instruction fidelity.

101 2.2 CONCEPT ERASURE

102 To mitigate safety risks in text-to-image diffusion models, such as the generation of NSFW or
 103 copyright-sensitive content, concept erasure (CE) has emerged as a more efficient and principled
 104 alternative to pre-training filtering (Rombach et al., 2022) or post-generation filtering (Rando et al.,
 105 2022). The goal is to remove the model’s ability to generate images containing undesired concepts
 106 while preserving its overall generative capacity. Existing methods typically align model outputs
 107 with and without concept-conditioned prompts. FMN (Zhang et al., 2024a) minimizes attention

activations associated with target concept text tokens. ESD (Gandikota et al., 2023) and CA (Kumari et al., 2023) fine-tune cross-attention modules by aligning predicted noise via MSE. UCE (Gandikota et al., 2024) solves a closed-form optimization of the text projection matrix. Subsequent works (Lu et al., 2024; Zhang et al., 2024c; Bui et al., 2024; Kim et al., 2024) leverage techniques such as LoRA and adversarial training to improve erasure precision while maintaining generation quality, and recent works (Zhang et al., 2025; Gao et al., 2025) have extended concept erasure to FLUX, a transformer-based diffusion model with flow matching. However, existing approaches are constrained to the diffusion paradigm and are not directly applicable to VAR models, which differ fundamentally in architecture and generation dynamics. This work identifies the key obstacles in adapting CE methods to VAR and introduces the first effective erasure method tailored for VAR models.

3 PRELIMINARIES

In autoregressive visual generation, the image is first encoded into a latent representation following a fixed raster scan manner and then quantized into a sequence of discrete tokens $t = \{t_1, t_2, \dots, t_N\}$. During inference, the model predicts the next visual token t_n conditioned on all previously generated tokens $t_{<n} = \{t_1, t_2, \dots, t_{n-1}\}$ and the condition c . The predicted probabilities of whole image can be formulated as follow:

$$p(x) = \prod_{n=1}^N p(t_n | t_{<n}, c). \quad (1)$$

VAR (Tian et al., 2024) redefines the autoregressive pipeline objective by predicting the next scale visual tokens. Given an image x , VAR first encodes it into continuous feature representations $f \in \mathbb{R}^{h \times w \times C}$, which are then quantized into a K level residual token maps $r = \{r_1, r_2, \dots, r_K\}$, each scale map r_i contains $h_i \times w_i$ tokens $t \in \mathbb{R}^{2 \times d}$, where d is the vocabulary size of the VQ-VAE. Based on this residual sequence, f_k at each scale k can be reconstructed as below:

$$f_k = \sum_{i=1}^K \text{upsample}(\text{lookup}(r_i)), \quad (2)$$

where $\text{upsample}(\cdot)$ refers to linear upsampling and $\text{lookup}(\cdot)$ refers to matching codebook. f_k at each level is the cumulative sum of lower-scale features. The visual transformer predicts the residuals r_k at the next scale, conditioned on the existing residual sequence $r_{<k} = \{r_1, r_2, \dots, r_{k-1}\}$ and condition c . The overall generation process can be formalized as follows.

$$p(r) = \prod_{i=1}^K p(r_i | r_{<i}, c), \quad (3)$$

To address the computational overhead associated with an expanded codebook, Infinity (Han et al., 2025) replaces the original vector quantizer in VAR with a bit-wise quantizer. For each input vector $z \in \mathbb{R}^d$, BSQ (Zhao et al., 2024) is applied to obtain a binary output q as defined below:

$$q = \frac{1}{\sqrt{d}} \text{sign}\left(\frac{z}{|z|}\right), \quad (4)$$

where $\text{sign}(\cdot)$ denotes the signum function. By transforming the prediction target into a bit-wise representation, Infinity successfully extends the VAR framework to large-scale text-to-image generation.

4 METHOD

In this section, we delve into the specifics of our method, aiming to address the limitations of directly applying diffusion-based CE methods to VAR models. The overall framework is shown in Figure 2.

4.1 VAR ERASURE FRAMEWORK WITH AUXILIARY VISUAL TOKENS

Diffusion-based CE methods align the predicted noise generated under prompt c^* which contains a target concept with the predicted noise generated under neutral prompts c which excludes the concept. This process can be formalized as follows.

$$\mathcal{L}_{era} = \mathbb{E}_t[||\epsilon_{\theta^*}(x_t, c^*, t) - \epsilon_{\theta}(x_t, c, t)||_2^2], \quad (5)$$

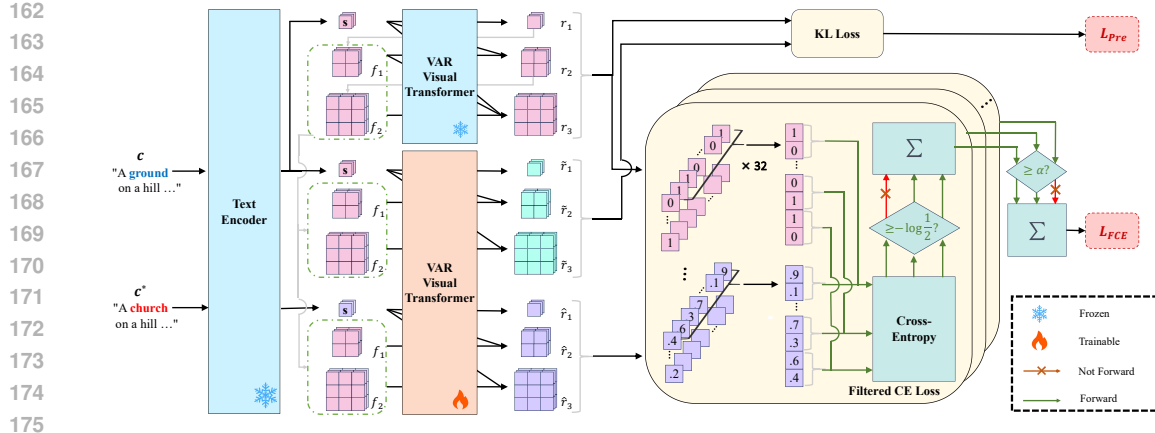


Figure 1: The framework of our method. The left part illustrates the proposed erasure framework adapted for VAR models, while the right part presents the proposed filtered cross entropy loss \mathcal{L}_{FCE} and the preservation loss \mathcal{L}_{Pre} .

where x_t denotes the noised latent at timestep t , θ^* and θ represent the trainable fine-tuned model parameters and original model parameters, respectively. A straightforward approach to adapting existing CE methods to the VAR framework is to replace the predicted noise x_t at each diffusion timestep in Eq. (5) with the predicted visual tokens r_i at each scale, as shown below:

$$\mathcal{L}_{vanilla} = \mathbb{E}_i[||p_{\theta^*}(r_i | r_{<i}, c^*) - p_{\theta}(r_i | r_{<i}, c)||_2^2], \quad (6)$$

However, unlike denoising models where denoising steps are relatively independent across timesteps, VAR generation is highly autoregressive: each token prediction depends heavily on previously predicted tokens at coarser scales. Consequently, optimization with Eq. (6) introduces errors that accumulate progressively across scales, eventually causing severe image quality collapse, as illustrated in the left column of Figure 2.

To mitigate this issue, we provide the VAR visual transformer with auxiliary visual tokens as additional inputs, which serve as references to stabilize generation. To further reduce the optimization search space, we incorporate tokens predicted by $p_{\theta}(r_i | r_{<i}, c^*)$ and $p_{\theta}(r_i | r_{<i}, c)$ during training, where $r_{ori,*}$ and r_{ori} denote the tokens generated from prompts c^* and c , respectively. As shown in the middle column of Figure 2, using $r_{ori,*}$ alleviates collapse to some extent, but large discrepancies between target and auxiliary tokens still prevent faithful generation. In contrast, when r_{ori} are provided (see left of Figure 1), the model only needs to adjust cross-attention responses to account for the effect of c^* , leaving the overall behavior largely intact. This enables accurate concept editing with minimal disruption, as demonstrated in the right column of Figure 2. Formally, the erasure loss of **VAR** is defined as:

$$\mathcal{L}_{VAR} = \mathbb{E}_i[||p_{\theta^*}(r_i | r_{<i}^{ori}, c^*) - p_{\theta}(r_i | r_{<i}^{ori}, c)||_2^2], \quad (7)$$

4.2 FILTERED CROSS ENTROPY LOSS FOR SURGICAL ERASURE

In Section 4.1, we introduced **VAR** and formulated an MSE-based loss that leverages auxiliary visual tokens as shown in Eq. (7). While this regression-style formulation is effective for diffusion models, where training aligns predicted noise with continuous reference signals, it is not directly applicable to autoregressive models such as **Infinity**, where predictions are defined over a discrete probability space. This fundamental mismatch leads to unstable optimization and severe semantic distortion in the generated images, often degrading the fidelity of the main subject.

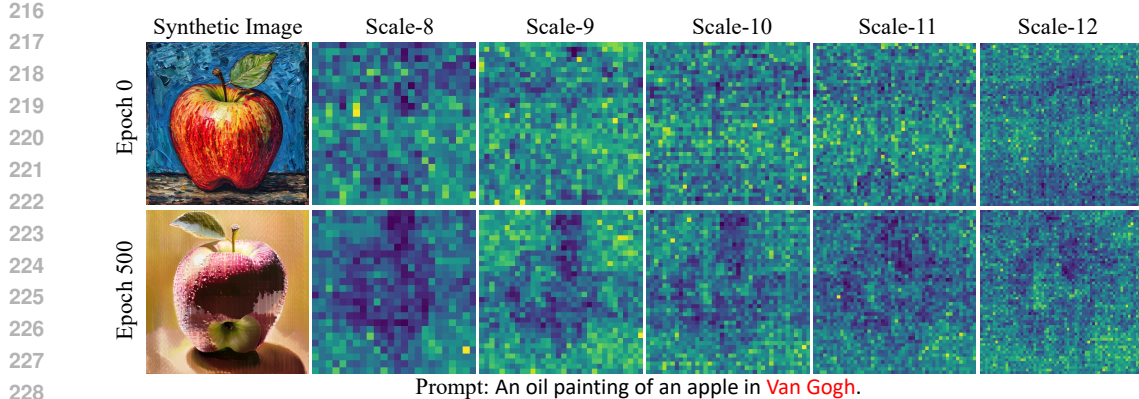


Figure 3: Heatmap visualizations of token-wise losses across different scales, the bluer color denotes the lower loss value. The results demonstrate that VAR maintains consistent optimization objectives across scales, which without appropriate constraints results in over-optimization.

To address this issue, we modify Eq. (7) to accommodate the prediction characteristics of Infinity. Specifically, BSQ is applied to all the visual tokens within $p_{\theta}(r_i | r_{<i}, c)$ predicted by the original model, and cross-entropy is used as the training loss, following the same paradigm as Infinity. However, during the optimization process, we observe that VAR models tend to produce consistent subject token alignment across scales, as shown in Figure 3, which can lead to over-optimization when early-stage representations exhibit significantly different patterns. To mitigate this, we employ a filtering strategy that performs filtering at two fine-grained levels. For the bit level, given that Infinity is optimized with a binary classification objective, it is natural to adopt binary classification accuracy $-\log \frac{1}{2}$ as the threshold γ . At this level, we obtain the prediction accuracy for each bit in one token. As for the token level, considering that Infinity is trained with 0%–30% bit-wise self-correction to enhance robustness to minor prediction errors (Han et al., 2025), we define a token as correct and exclude it from the loss computation if the percentage of incorrect bits is less than α . We obtain the mask F_i to reduce the optimization strength to the correct tokens in the i -th scale as follows:

$$\mathcal{L}_{CE} = \log p_{\theta^*}(r_i | r_{<i}^{ori}, c^*) \quad (8)$$

$$F_i = \mathbb{I}(\text{ratio}(\mathcal{L}_{CE} \geq \gamma) > \alpha) \quad (9)$$

where $\mathcal{L}_{CE}(\cdot) \in \mathbb{R}^{h_i \times w_i \times d}$ represents the loss function in the i -th scale calculated by binary cross entropy, $\text{ratio}(\cdot)$ denotes the percentage of the correct dimensions within tokens and $\mathbb{I}(m > \alpha)$ is an indicator function which yields a value of 1 if $m > \alpha$ and 0 otherwise, and we set α as 25% to be consistent with the original self-correction range. The overall filtered cross entropy function is formalized as follows:

$$\mathcal{L}_{FCE} = \sum_{i=1}^K F_i \odot \log p_{\theta^*}(r_i | r_{<i}^{ori}, c^*), \quad (10)$$

where F_i represents the token-wise filter applied on the token map r_i at scale i . The detailed process of Eq. (10) is presented in the right part of Figure 1.

4.3 IRRELEVANT CONCEPT PRESERVATION LOSS

Existing diffusion-based CE methods have introduced various preservation strategies such as restricting the optimized parameters (Fan et al., 2023), employing adversarial training (Bui et al., 2025), and incorporating contrastive learning loss (Gao et al., 2025) to mitigate semantic drift and the reduction of diversity caused by repeatedly aligning specific concepts during fine-tuning. However, similar to the erasure losses that cannot be directly applied to the VAR framework, these preservation strategies are also not directly transferable.

To address this limitation, we propose a novel preservation loss for alignment. Specifically, we use c as the prompt for the fine-tuned model and align its output $p_{\theta^*}(r_i | r_{<i}^{ori}, c)$ with $p_{\theta}(r_i | r_{<i}^{ori}, c)$ predicted by the original model. In this way, the fine-tuned model imitates the generation behavior of

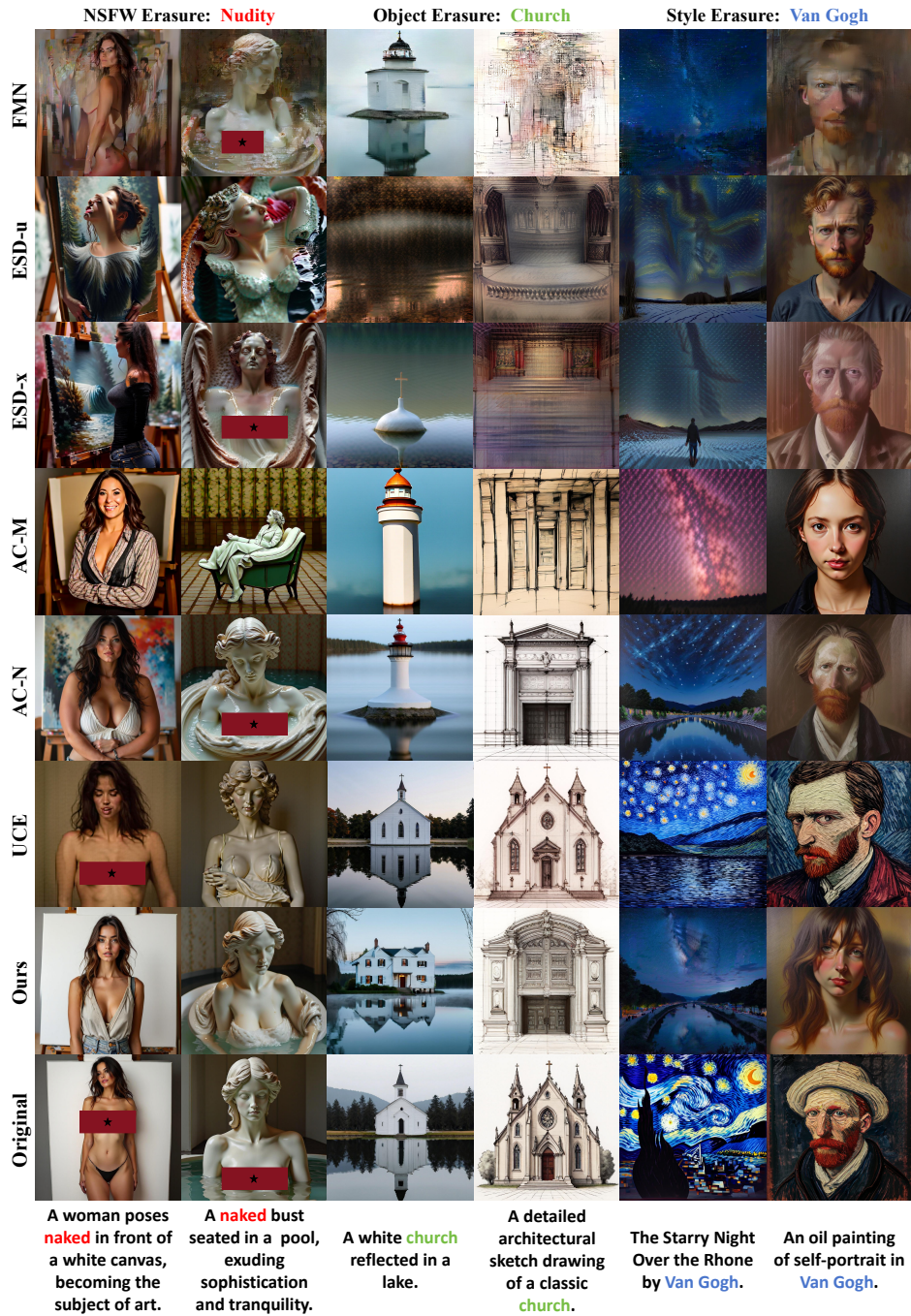


Figure 4: Generated images from the **S-VARE** and other baselines which are applied on **VAR**. Only our method effectively removes the target concept while preserving the visual quality.

the teacher model at each scale, thereby preserving the overall generative capability. To maximize the similarity between the probability distributions of the different models, we adopt the KL divergence $D_{KL}(\cdot \parallel \cdot)$ as the loss function which could be formalized as below:

$$\mathcal{L}_{Pre} = \sum_{i=1}^K D_{KL}(p_{\theta}(r_i \mid r_{<i}^{ori}, c) \parallel p_{\theta^*}(r_i \mid r_{<i}^{ori}, c)). \quad (11)$$

The final optimization target could be formulated as $\mathcal{L}_{FCE} + \mathcal{L}_{Pre}$, with each term assigned equal weight, achieving surgical concept erasure while preserving the overall generative capacity.

324
 325 Table 1: Quantitative comparison across three common concept erasure types. Our method eliminates
 326 the target concepts while preserving the overall generative capability of the model, achieving surgical
 327 and effective concept erasure.

Method	NSFW Erasure				Object Erasure				Style Erasure		
	Sen.↓	Com.↑	FID↓	CLIP↑	ACC _e (%) ↓	ACC _i (%) ↑	FID↓	CLIP↑	ACC(%)↓	FID↓	CLIP↑
Original	158	112	31.1	31.7	94.2	76.0	31.1	31.7	76.0	31.1	31.7
UCE	122	100	37.8	26.4	92.8	71.2	33.7	29.9	68.2	33.8	29.3
FMN	22	8	35.4	28.2	12.2	60.5	37.5	30.2	34.4	34.7	29.6
ESD-u	21	2	34.5	30.3	4.2	50.3	34.4	29.8	14.6	34.0	29.2
ESD-x	26	6	33.8	29.9	3.8	58.1	34.9	30.4	16.2	33.2	30.3
AC-M	20	10	34.7	28.8	8.2	66.2	36.1	29.4	12.8	33.4	29.7
AC-N	32	34	33.7	30.2	9.8	68.9	35.3	30.6	18.4	34.1	30.5
Ours	5	57	32.8	31.3	4.4	75.7	31.5	31.6	8.2	32.1	31.5

337 5 EXPERIMENT

339 5.1 IMPLEMENTATION DETAILS

341 **Model and Datasets.** We adopt Infinity-2B (Han et al., 2025), currently the only publicly available
 342 VAR model that supports large-scale text-to-image generation, as the base architecture and finetune
 343 the FFN and Cross-attention modules. For training data construction, we follow the ECGVF (Fan
 344 et al., 2025) benchmark and employ a large language model (LLM) to generate natural language
 345 prompt pairs. Each pair consists of one prompt containing the target concept to be erased and a
 346 corresponding semantically consistent prompt in which the target concept is replaced by other words,
 347 please refer to Appendix D for more details. For test data, we follow the design in (Zhang et al.,
 348 2025) and use the GPT-4o model (Hurst et al., 2024) to generate prompts of varying lengths that
 349 explicitly include the target concept. These test prompts are not included in the training set. To
 350 evaluate robustness, we use the adversarial datasets Ring-A-Bell (R-A-B) (Tsai et al., 2023) and
 351 MMA (Yang et al., 2024), as well as the real-user prompt dataset I2P (Schramowski et al., 2023).

352 **Baselines.** We adapt several representative CE methods originally developed for diffusion models and
 353 use them as baselines, including ESD (Gandikota et al., 2023), AC (Kumari et al., 2023), FMN (Zhang
 354 et al., 2024a), and UCE (Gandikota et al., 2024), covering all categories of loss functions employed
 355 in existing CE approaches. It is important to note that these methods must also be deployed within
 356 our proposed **VARE** framework in order to enable fine-tuning; otherwise, they cannot be applied to
 357 VAR models. Consequently, the only difference between these converted baselines and our proposed
 358 **S-VARE** lies in the choice of loss function and more details are provided in Appendix A.

359 **Evaluation Metrics.** For NSFW erasure, we employ NudeNet (Bedapudi, 2022) as the classifier.
 360 The evaluation metrics include the number of sensitive content (Sen.↓), e.g., female breast, and the
 361 number of common content (Com.↑), e.g., feet. For object erasure, we use an ImageNet-1K pretrained
 362 ResNet-50 (He et al., 2016) as the classifier. The metrics include the classification accuracy of images
 363 corresponding to the erased concept class (ACC_e ↓) and that of images corresponding to other
 364 irrelevant concept class (ACC_i ↑). For style erasure, we apply a pre-trained style detector (Zhang
 365 et al., 2024d) to assess whether the erased style appears in generated images (ACC↓). We compute the
 366 CLIP score and FID on the COCO-30K (Lin et al., 2014) to assess the overall generative capability
 367 of all erased models.

368 5.2 MAIN RESULTS

370 Figure 4 and Table 1 present the comparison results for three concept erasure types: NSFW erasure,
 371 object erasure, and style erasure. We discuss the results in the following. For more visualizations,
 372 please refer to Appendix E.

373 **NSFW erasure.** We select “naked” as the target NSFW concept which is the mostly considered
 374 harmful concept, our method achieves nearly complete erasure, as shown in Table 1. To evaluate the
 375 preservation of general content, we use the generation of normal body parts without pornography as
 376 an indicator. The results show that our method performs only below UCE, which exhibits almost no
 377 erasure effect, while substantially outperforming other methods whose generation quality severely
 degrades, as illustrated in Figure 4.

378
379 Table 2: The performance of our method on erasing different classes in Imagenette. Our method
380 achieves effective erasure performance while having minimal impact on the irrelevant objects.
381

Object	ACC _e (%)		ACC _i (%)		FID		CLIP	
	Origin	Ours	Origin	Ours	Origin	Ours	Origin	Ours
Cassette Player	99.0	3.8	75.5	75.1	-	32.4	-	31.7
Chain Saw	95.0	2.5	76.0	75.2	-	31.8	-	31.4
Church	94.2	4.4	76.0	75.7	-	31.5	-	31.6
Gas Pump	95.4	5.0	75.9	74.5	-	33.0	-	31.1
Tench	62.8	1.2	79.5	78.8	-	32.7	-	31.4
Garbage Truck	95.2	4.2	75.9	74.1	-	33.2	-	31.2
English Springer	16.4	0.0	84.7	82.5	-	31.6	-	31.3
Golf Ball	100.0	2.1	75.4	75.0	-	31.4	-	31.5
Parachute	100.0	1.8	75.4	74.8	-	31.8	-	31.5
French Horn	20.6	0.0	84.2	83.8	-	31.6	-	31.6
Average	77.9	2.5	77.9	76.9	31.1	32.1	31.7	31.4



407 Figure 5: The images generated by different
408 methods with adversarial prompt.
409

395
396
397
398
399
400 Table 3: The nudity erasure performance of our
401 method under adversarial prompts. We successfully
402 reduce the the attack success rate of the adversarial
403 prompts, showing the potential to serve as an effec-
404 tive defense mechanism.
405

Dataset	Sen.↓		ASR (%)↓		Com.-	
	Origin	Ours	Origin	Ours	Origin	Ours
I2P	362	97	4.1	0.8	419	146
MMA	441	101	21.7	3.5	477	184
R-A-B	168	24	75.9	7.4	105	52
Normal	158	5	53.0	3.0	112	57

410 For prompts with more fine-grained descriptions, such as “... exuding sophistication and tranquility,”
411 only our method is able to accurately translate them into corresponding images. Moreover, when
412 compared with images generated by the original model, the outputs of our method preserve the overall
413 structure with minimal differences, apart from the erased concept.
414

415 **Object erasure.** We select the most used “church” as the target concept to erasure. As shown in
416 Table 1, compared to the most powerful method ESD which disruptively alters the model’s generative
417 performance, the erasure performance our method is slightly lower yet the preservation performance
418 irrelevant classes is outstanding.
419

420 In Table 2, we further present the results across different classes in ImageNet. It can be observed
421 that, regardless of whether the original model can accurately generate images of the target class, our
422 method achieves near-complete erasure of the target concept while preserving overall generative
423 performance with minimal degradation.
424

425 **Style erasure.** We select “Van Gogh” as the target artistic style, where our method also achieves
426 effective erasure. However, since the evaluation data contain painting-related prompts such as “An
427 oil painting of ...”, our method could occasionally be detected as a specific artistic style. As shown
428 in Figure 4, other baselines often produce distorted strokes and artifacts, indicating a decline in the
429 model’s generative capability. In contrast, our method faithfully adheres to the requirements of the
430 prompts and is still capable of producing natural images with clear semantic information.
431

432 **Robustness evaluation.** To further validate the robustness of our method, we evaluate the erased
433 model using adversarial datasets specifically designed to induce nudity concept. Since no adversarial
434 attack benchmark currently exists for VAR models, we directly adopt publicly available adversarial
435 prompt datasets originally developed for diffusion models. As shown in Table 3, although these
436



Figure 6: The visual performance of each component.

adversarial samples are not included in our training data, our method still substantially reduces the generation of nudity features and effectively lowers the adversarial success rate (ASR).

The qualitative comparisons with other baselines presented in Figure 5 further highlight the advantage of our method. Our method produces images that remove sensitive contents while preserving semantic consistency with the original model. In contrast, other methods, particularly UCE, exhibit noticeable degradation in visual quality, indicating that these approaches excessively disrupt the model’s generative patterns.

5.3 ABLATION STUDY

Efficacy of the loss function. We take Eq. (7) as our baseline and conduct ablation study on the two proposed loss functions included in **S-VARE**. As shown in Table 4, we report the quantitative results on erasing the “church”. Incorporating \mathcal{L}_{FCE} effectively strengthens the erasure performance, and adding \mathcal{L}_{Pre} on top of it further improves the generative quality of the model. As illustrated in Figure 6, we present qualitative results on different concept erasure tasks. The results show that \mathcal{L}_{FCE} successfully eliminates visual collapse, while \mathcal{L}_{Pre} further enhances instruction fidelity. We provided more ablation study in Appendix C.3 and C.2.

Impact of the filter ratio. We further validate the effectiveness of our proposed filtering strategy of the \mathcal{L}_{FCE} on challenging nudity erasure. A larger value of α indicates that a token must contain more erroneous bits to be included in the loss computation as shown in Eq. (8), which typically weakens the optimization strength of the model. As shown in Table 5, increasing α results in a gradual rise in ASR, while perceptual metrics of generation quality improve, demonstrating the effectiveness of the filter. In practice, we select a balanced threshold of 25% as the default parameter for all the tasks.

6 CONCLUSION

In this work, we present the first effective framework for concept erasure in VAR-based text-to-image models, addressing the critical gap left by diffusion-oriented methods that do not transfer well to autoregressive architectures. We introduce **VARE**, which mitigates error accumulation by incorporating auxiliary visual tokens, and further propose **S-VARE**, a surgical erasure approach that combines a filtered cross-entropy loss with a preservation loss tailored to VAR models. Extensive experiments demonstrate that our approach achieves precise and reliable concept erasure while maintaining the overall generative capacity of the model.

Table 4: Quantitative results of the two proposed loss function. \mathcal{L}_{FCE} enhances both erasure effectiveness and generation quality through precise control, while \mathcal{L}_{Pre} further improves generation quality with negligible impact on erasure capability.

	ACC _e ↓	ACC _i ↑	FID ↓	CLIP↑
Baseline	9.8	68.9	35.3	30.6
+ \mathcal{L}_{FCE}	4.1	73.5	32.4	31.2
+ \mathcal{L}_{Pre}	4.4	75.7	31.5	31.6

Table 5: Ablation study on the ratio threshold α of selected bits on Ring-A-Bell dataset.

α (%)	ASR (%)↓	FID↓	CLIP↑
0	7.2	33.6	30.9
25	7.4	32.8	31.3
50	21.7	32.9	31.2
75	40.2	31.4	31.5

486 REFERENCES
487

488 Praneeth Bedapudi. Nudenet: lightweight nudity detection. <https://github.com/notAI-tech/NudeNet>, 2022. Accessed: 2025-06-25.

490 Anh Bui, Long Vuong, Khanh Doan, Trung Le, Paul Montague, Tamas Abraham, and Dinh Phung.
491 Erasing undesirable concepts in diffusion models with adversarial preservation. In *Advances in
492 Neural Information Processing Systems*, volume 37, pp. 133112–133146, 2024.

493 Anh Bui, Trang Vu, Long Vuong, Trung Le, Paul Montague, Tamas Abraham, Junae Kim, and Dinh
494 Phung. Fantastic targets for concept erasure in diffusion models and where to find them. *arXiv
495 preprint arXiv:2501.18950*, 2025.

496 Minwoo Byeon, Beomhee Park, Haecheon Kim, Sungjun Lee, Woonhyuk Baek, and Sae-
497 hoon Kim. Coyo-700m: Image-text pair dataset. [https://github.com/kakaobrain/
498 coyo-dataset](https://github.com/kakaobrain/coyo-dataset), 2022.

499 Ruchika Chavhan, Da Li, and Timothy Hospedales. Conceptprune: Concept editing in diffusion
500 models via skilled neuron pruning. *arXiv preprint arXiv:2405.19237*, 2024.

501 Xiaokang Chen, Zhiyu Wu, Xingchao Liu, Zizheng Pan, Wen Liu, Zhenda Xie, Xingkai Yu, and
502 Chong Ruan. Janus-pro: Unified multimodal understanding and generation with data and model
503 scaling. *arXiv preprint arXiv:2501.17811*, 2025.

504 Chaorui Deng, Deyao Zhu, Kunchang Li, Chenhui Gou, Feng Li, Zeyu Wang, Shu Zhong, Weihao
505 Yu, Xiaonan Nie, Ziang Song, et al. Emerging properties in unified multimodal pretraining. *arXiv
506 preprint arXiv:2505.14683*, 2025.

507 Chongyu Fan, Jiancheng Liu, Yihua Zhang, Eric Wong, Dennis Wei, and Sijia Liu. Salun: Em-
508 powering machine unlearning via gradient-based weight saliency in both image classification and
509 generation. *arXiv preprint arXiv:2310.12508*, 2023.

510 Haipeng Fan, Shiyuan Zhang, Zihang Guo, Huaiwen Zhang, et al. Ear: Erasing concepts from unified
511 autoregressive models. *arXiv preprint arXiv:2506.20151*, 2025.

512 Lijie Fan, Tianhong Li, Siyang Qin, Yuanzhen Li, Chen Sun, Michael Rubinstein, Deqing Sun,
513 Kaiming He, and Yonglong Tian. Fluid: Scaling autoregressive text-to-image generative models
514 with continuous tokens. *arXiv preprint arXiv:2410.13863*, 2024.

515 Rohit Gandikota, Joanna Materzynska, Jaden Fiotto-Kaufman, and David Bau. Erasing concepts
516 from diffusion models. In *Proceedings of the IEEE/CVF International Conference on Computer
517 Vision*, pp. 2426–2436, 2023.

518 Rohit Gandikota, Hadas Orgad, Yonatan Belinkov, Joanna Materzyńska, and David Bau. Unified
519 concept editing in diffusion models. In *Proceedings of the IEEE/CVF Winter Conference on
520 Applications of Computer Vision*, pp. 5111–5120, 2024.

521 Daiheng Gao, Shilin Lu, Wenbo Zhou, Jiaming Chu, Jie Zhang, Mengxi Jia, Bang Zhang, Zhaoxin
522 Fan, and Weiming Zhang. Eraseanything: Enabling concept erasure in rectified flow transformers.
523 In *Forty-second International Conference on Machine Learning*, 2025.

524 Jian Han, Jinlai Liu, Yi Jiang, Bin Yan, Yuqi Zhang, Zehuan Yuan, Bingyue Peng, and Xiaobing
525 Liu. Infinity: Scaling bitwise autoregressive modeling for high-resolution image synthesis. In
526 *Proceedings of the Computer Vision and Pattern Recognition Conference*, pp. 15733–15744, 2025.

527 Kaiming He, Xiangyu Zhang, Shaoqing Ren, and Jian Sun. Deep residual learning for image
528 recognition. In *Proceedings of the IEEE conference on computer vision and pattern recognition*,
529 pp. 770–778, 2016.

530 Edward J Hu, Yelong Shen, Phillip Wallis, Zeyuan Allen-Zhu, Yuanzhi Li, Shean Wang, Lu Wang,
531 Weizhu Chen, et al. Lora: Low-rank adaptation of large language models. *ICLR*, 1(2):3, 2022.

532 Aaron Hurst, Adam Lerer, Adam P Goucher, Adam Perelman, Aditya Ramesh, Aidan Clark, AJ Os-
533 trow, Akila Welihinda, Alan Hayes, Alec Radford, et al. Gpt-4o system card. *arXiv preprint
534 arXiv:2410.21276*, 2024.

540 Harry H Jiang, Lauren Brown, Jessica Cheng, Mehtab Khan, Abhishek Gupta, Deja Workman, Alex
 541 Hanna, Johnathan Flowers, and Timnit Gebru. Ai art and its impact on artists. In *Proceedings of*
 542 *the 2023 AAAI/ACM Conference on AI, Ethics, and Society*, pp. 363–374, 2023.

543 Changhoon Kim, Kyle Min, and Yezhou Yang. Race: Robust adversarial concept erasure for
 544 secure text-to-image diffusion model. In *European Conference on Computer Vision*, pp. 461–478.
 545 Springer, 2024.

546 Nupur Kumari, Bingliang Zhang, Sheng-Yu Wang, Eli Shechtman, Richard Zhang, and Jun-Yan
 547 Zhu. Ablating concepts in text-to-image diffusion models. In *Proceedings of the IEEE/CVF*
 548 *International Conference on Computer Vision*, pp. 22691–22702, 2023.

549 Black Forest Labs. Flux. <https://github.com/black-forest-labs/flux>, 2024.

550 Xiang Li, Kai Qiu, Hao Chen, Jason Kuen, Zhe Lin, Rita Singh, and Bhiksha Raj. Controlvar:
 551 Exploring controllable visual autoregressive modeling. *arXiv preprint arXiv:2406.09750*, 2024.

552 Tsung-Yi Lin, Michael Maire, Serge Belongie, James Hays, Pietro Perona, Deva Ramanan, Piotr
 553 Dollár, and C Lawrence Zitnick. Microsoft coco: Common objects in context. In *European*
 554 *conference on computer vision*, pp. 740–755. Springer, 2014.

555 Yaron Lipman, Ricky TQ Chen, Heli Ben-Hamu, Maximilian Nickel, and Matt Le. Flow matching
 556 for generative modeling. *arXiv preprint arXiv:2210.02747*, 2022.

557 Shilin Lu, Zilan Wang, Leyang Li, Yanzhu Liu, and Adams Wai-Kin Kong. Mace: Mass concept
 558 erasure in diffusion models. In *Proceedings of the IEEE/CVF Conference on Computer Vision and*
 559 *Pattern Recognition*, pp. 6430–6440, 2024.

560 Yiting Qu, Xinyue Shen, Xinlei He, Michael Backes, Savvas Zannettou, and Yang Zhang. Unsafe
 561 diffusion: On the generation of unsafe images and hateful memes from text-to-image models. In
 562 *Proceedings of the 2023 ACM SIGSAC conference on computer and communications security*, pp.
 563 3403–3417, 2023.

564 Aditya Ramesh, Prafulla Dhariwal, Alex Nichol, Casey Chu, and Mark Chen. Hierarchical text-
 565 conditional image generation with clip latents. *arXiv preprint arXiv:2204.06125*, 1(2):3, 2022.

566 Javier Rando, Daniel Paleka, David Lindner, Lennart Heim, and Florian Tramèr. Red-teaming the
 567 stable diffusion safety filter. *arXiv preprint arXiv:2210.04610*, 2022.

568 Robin Rombach, Andreas Blattmann, Dominik Lorenz, Patrick Esser, and Björn Ommer. High-
 569 resolution image synthesis with latent diffusion models. In *Proceedings of the IEEE/CVF confer-*
 570 *ence on computer vision and pattern recognition*, pp. 10684–10695, 2022.

571 Olaf Ronneberger, Philipp Fischer, and Thomas Brox. U-net: Convolutional networks for biomedical
 572 image segmentation. In *Medical image computing and computer-assisted intervention—MICCAI*
 573 *2015: 18th international conference, Munich, Germany, October 5–9, 2015, proceedings, part III*
 574 *18*, pp. 234–241. Springer, 2015.

575 Patrick Schramowski, Manuel Brack, Björn Deiseroth, and Kristian Kersting. Safe latent diffusion:
 576 Mitigating inappropriate degeneration in diffusion models. In *Proceedings of the IEEE/CVF*
 577 *Conference on Computer Vision and Pattern Recognition*, pp. 22522–22531, 2023.

578 Christoph Schuhmann, Romain Beaumont, Richard Vencu, Cade Gordon, Ross Wightman, Mehdi
 579 Cherti, Theo Coombes, Aarush Katta, Clayton Mullis, Mitchell Wortsman, et al. Laion-5b: An
 580 open large-scale dataset for training next generation image-text models. *Advances in neural*
 581 *information processing systems*, 35:25278–25294, 2022.

582 Keyu Tian, Yi Jiang, Zehuan Yuan, Bingyue Peng, and Liwei Wang. Visual autoregressive modeling:
 583 Scalable image generation via next-scale prediction. *Advances in neural information processing*
 584 *systems*, 37:84839–84865, 2024.

585 Yu-Lin Tsai, Chia-Yi Hsu, Chulin Xie, Chih-Hsun Lin, Jia-You Chen, Bo Li, Pin-Yu Chen, Chia-Mu
 586 Yu, and Chun-Ying Huang. Ring-a-bell! how reliable are concept removal methods for diffusion
 587 models? *arXiv preprint arXiv:2310.10012*, 2023.

594 Aaron Van Den Oord, Oriol Vinyals, et al. Neural discrete representation learning. *Advances in*
 595 *neural information processing systems*, 30, 2017.

596

597 Ashish Vaswani, Noam Shazeer, Niki Parmar, Jakob Uszkoreit, Llion Jones, Aidan N Gomez, Łukasz
 598 Kaiser, and Illia Polosukhin. Attention is all you need. *Advances in neural information processing*
 599 *systems*, 30, 2017.

600

601 Xinlong Wang, Xiaosong Zhang, Zhengxiong Luo, Quan Sun, Yufeng Cui, Jinsheng Wang, Fan
 602 Zhang, Yueze Wang, Zhen Li, Qiyi Yu, et al. Emu3: Next-token prediction is all you need.
arXiv preprint arXiv:2409.18869, 2024a.

603

604 Yuqing Wang, Tianwei Xiong, Daquan Zhou, Zhijie Lin, Yang Zhao, Bingyi Kang, Jiashi Feng, and
 605 Xihui Liu. Loong: Generating minute-level long videos with autoregressive language models.
arXiv preprint arXiv:2410.02757, 2024b.

606

607 Yijun Yang, Ruiyuan Gao, Xiaosen Wang, Tsung-Yi Ho, Nan Xu, and Qiang Xu. Mma-diffusion:
 608 Multimodal attack on diffusion models. In *Proceedings of the IEEE/CVF Conference on Computer*
 609 *Vision and Pattern Recognition*, pp. 7737–7746, 2024.

610

611 Ziyu Yao, Jialin Li, Yifeng Zhou, Yong Liu, Xi Jiang, Chengjie Wang, Feng Zheng, Yuexian Zou,
 612 and Lei Li. Car: Controllable autoregressive modeling for visual generation. *arXiv preprint*
arXiv:2410.04671, 2024.

613

614 Qihang Yu, Ju He, Xueqing Deng, Xiaohui Shen, and Liang-Chieh Chen. Randomized autoregressive
 615 visual generation. *arXiv preprint arXiv:2411.00776*, 2024.

616

617 Gong Zhang, Kai Wang, Xingqian Xu, Zhangyang Wang, and Humphrey Shi. Forget-me-not:
 618 Learning to forget in text-to-image diffusion models. In *Proceedings of the IEEE/CVF conference*
on computer vision and pattern recognition, pp. 1755–1764, 2024a.

619

620 Qian Zhang, Xiangzi Dai, Ninghua Yang, Xiang An, Ziyong Feng, and Xingyu Ren. Var-clip:
 621 Text-to-image generator with visual auto-regressive modeling. *arXiv preprint arXiv:2408.01181*,
 622 2024b.

623

624 Yang Zhang, Er Jin, Yanfei Dong, Yixuan Wu, Philip Torr, Ashkan Khakzar, Johannes Stegmaier,
 625 and Kenji Kawaguchi. Minimalist concept erasure in generative models. *arXiv preprint*
arXiv:2507.13386, 2025.

626

627 Yimeng Zhang, Xin Chen, Jinghan Jia, Yihua Zhang, Chongyu Fan, Jiancheng Liu, Mingyi Hong,
 628 Ke Ding, and Sijia Liu. Defensive unlearning with adversarial training for robust concept erasure
 629 in diffusion models. *Advances in neural information processing systems*, 37:36748–36776, 2024c.

630

631 Yimeng Zhang, Jinghan Jia, Xin Chen, Aochuan Chen, Yihua Zhang, Jiancheng Liu, Ke Ding, and
 632 Sijia Liu. To generate or not? safety-driven unlearned diffusion models are still easy to generate
 633 unsafe images... for now. In *European Conference on Computer Vision*, pp. 385–403. Springer,
 634 2024d.

635

636 Yue Zhao, Yuanjun Xiong, and Philipp Krähenbühl. Image and video tokenization with binary
 637 spherical quantization. *arXiv preprint arXiv:2406.07548*, 2024.

638

639

640

641

642

643

644

645

646

647

648
649

APPENDIX

650
651

A DISCUSSION ON ADAPTING DIFFUSION-BASED METHODS TO VAR

652
653
654
655

FMN (Zhang et al., 2024a). We employ hooks to extract the attention activation A of all cross-attention (CA) modules and minimize intermediate attention maps associated with the target concepts to forget using the L2 norm proposed in the original paper, which could be formulated as follow:

656
657

$$\mathcal{L}_{FMN} = \sum_{a_t \in A_t} \|a_t^p\|^2, \quad (12)$$

658
659
660
661
662

where a_t^p represents the activation belongs to A at timestep t and position p , and p is the location of the target concept words in the prompt. We adopt the same parameter settings and finetune both the feed-forward networks (FFN) and CA modules. However, the results in Figure 4 show that simply minimizing the CA outputs severely degrades image generation quality, leading to pronounced artifacts and color blocking.

663
664

ESD-u (Gandikota et al., 2023). ESD derives its loss function from the classifier-free guidance (CFG) formulation according to the requirements of the concept erasure task as shown below:

665

$$\mathcal{L}_{ESD} = \mathbb{E}_i[\|p_{\theta^*}(r_i | r_{<i}^{ori}, c^*) - p_{\theta}(r_i | r_{<i}^{ori}, c) + \eta[p_{\theta}(r_i | r_{<i}^{ori}, c^*) - p_{\theta}(r_i | r_{<i}^{ori}, c)]\|_2^2]. \quad (13)$$

666
667
668
669
670
671
672

However, unlike diffusion models, where differences can be directly computed on the predicted noise and denoising steps are relatively independent, Infinity predicts bit values in the probability space. Subtracting or adding visual tokens often leads to generation collapse, as illustrated in Figure 4. Following the configuration in the original paper, we set $\eta = 1$ and deploy Eq. (13) on **VAR**. ESD-u is a variation proposed in the original paper, optimizes all modules except CA. For consistency with our optimization parameters, we set the optimization targets to Self-attention modules (SA) and FFN.

673
674
675

ESD-x (Gandikota et al., 2023). The same loss function Eq. (13) as in ESD-u is used, with the only difference that ESD-x optimizes the CA modules. For consistency with our work, we set the optimization targets to both CA and FFN.

676
677
678
679
680

AC-M (Kumari et al., 2023). AC-M and ESD share the same optimization objective, namely aligning the predicted noise generated under prompts c^* containing the target concept with that generated under prompts c without the concept. Unlike ESD, which relies on a pretrained teacher model, AC performs training solely with the fine-tuned erasure model itself and therefore does not employ the CFG regularization term used in ESD. The formulation is given as follows.

681
682

$$\mathcal{L}_{AC-M} = \mathbb{E}_i[\|p_{\theta^*}(r_i | r_{<i}^{ori}, c^*) - p_{\theta^*}(r_i | r_{<i}^{ori}, c)\|_2^2]. \quad (14)$$

683
684
685
686
687

AC-N (Kumari et al., 2023). AC-N is a lightweight deployment variant of AC-M. Based on the principle that diffusion models predict the corresponding noise conditioned on prompts c^* containing specific concepts and subsequently perform denoising, AC-N proposes to directly align the model’s predicted noise under condition c^* with Gaussian noise to achieve concept erasure. This can be formalized as follows.

688

$$\mathcal{L}_{AC-N} = \mathbb{E}_i[\|p_{\theta^*}(r_i | r_{<i}^{ori}, c^*) - \epsilon\|_2^2]. \quad (15)$$

689
690
691
692
693
694

where ϵ denotes the gaussian noise. However, when this loss function is applied to VAR, the fine-tuned model loses its text-to-image generation capability, which is attributed to the fundamentally different inference mechanisms of visual autoregressive and diffusion models. To address this, we instead use the visual tokens generated by the teacher model under condition c as the prediction targets, as formulated in Eq. (7). Consequently, CA-N serves as the baseline deployed within the VARE framework in our ablation studies.

695
696
697

UCE (Gandikota et al., 2024). Unlike other concept erasure methods, UCE computes closed-form solutions for updating the parameters W_k and W_v in the attention modules, thereby achieving concept erasure without explicit optimization. This process is formulated as follows:

698
699
700

$$W^* = (\sum_{c^*} Wc(c^*)^T + \sum_c Wcc^T)(\sum_{c^*} c^*(c^*)^T + \sum_c cc^T)^{-1}. \quad (16)$$

701

However, when applying Eq. (16) to VAR models, we observe that it almost entirely fails to achieve effective erasure as shown in Table 1. We attribute this failure to the strong robustness of the T5 text

encoder and the visual Transformer used in VAR models against perturbations in word embeddings, which prevents successful erasure. Therefore, although UCE can be deployed efficiently, it cannot serve as a competitive baseline.

B DETAILED TRAINING SETTINGS

Table 6 reports the influential parameters involved in the training process. We employ the same parameter settings across all erasure tasks, further demonstrating the robustness of our method.

Table 6: Parameter setting of training the erased model across all the erasure tasks.

Parameter	Value
Batch size	2
Training prompt pairs	50
Training iterations	500
Preservation loss weight	1
Quantization precision	bf16
Finetuned parameter	CA + FFN
Optimizer	AdamW
β_0	0.9
β_1	0.95
Learning rate	2×10^{-3}
VAR pretrained weight	Infinity-2B
VQ-VAE vocabulary size	32
Resolution	1024×1024
Hardware	1 × NVIDIA A6000

C MORE QUANTITATIVE RESULTS

C.1 MULTIPLE CONCEPT ERASURE PERFORMANCE

To investigate whether our method can be extended to multi-concept erasure tasks, we design experiments that simultaneously erase multiple Imagenette classes, as shown in Table 7. The numbers indicate the count of classes erased simultaneously, with the set of classes progressively expanded in the order listed in Table 2 up to 10. Avg 10 denotes the average performance when each class is erased independently. The results show that, although erasing multiple concepts simultaneously leads to some degradation in both erasure performance and generative capability, our method remains largely unaffected due to its precise targeting of the concepts to be erased.

Table 7: Multiple concept erasure performance on erasing the class in ImageNette.

Number of concepts	ACC _e (%) ↓	FID↓	CLIP↑
1	3.8	32.4	31.7
2	3.5	32.7	31.4
5	4.0	33.1	31.3
10	3.7	34.2	30.8
Avg 10	2.5	32.1	31.4

Table 8: Ablation study on the selection of optimization parameters in nudity erasure.

	ASR(%)↓	FID↓	CLIP↑
SA	13.7	33.5	29.8
CA	9.1	33.9	30.7
SA + FFN	10.2	33.5	30.0
CA + FFN	7.4	32.8	31.3
SA + CA + FFN	7.1	33.1	31.0

C.2 ABLATION STUDY ON SELECTING OPTIMIZED MODULE

In our experiment setting, we select the parameters of the CA and FFN modules as optimization targets. To justify this choice, we design additional ablation studies. When optimizing only the SA or FFN parameters, we observe that the model fails to achieve effective erasure for more complex prompts. By contrast, optimizing the CA parameters leads to stronger erasure performance, as CA governs text–image interactions and thus responds more effectively to \mathcal{L}_{FCE} with different prompts



Figure 7: Visual samples with different optimized modules.

c and c^* . However, because CA responds weakly to \mathcal{L}_{Pre} with the same prompt c , the resulting images often deviate significantly from those of the original model.

Considering these factors, we adopt an optimization strategy that combines CA with FFN to stabilize the training process, as illustrated in Figure 7. We further experimented with including SA as an additional optimization target. As shown in Table 8, although this yields slightly stronger erasure performance, it also introduces more substantial degradation in generative quality and higher computational overhead due to the larger number of parameters being updated. Therefore, we ultimately choose to optimize only the CA and FFN parameters.

C.3 ABLATION STUDY ON EXCHANGING LOSS FUNCTION

Based on the generative characteristics of the Infinity model, we design the cross-entropy based \mathcal{L}_{FCE} as the erasure loss and the KL-divergence-based \mathcal{L}_{Pre} as the preservation loss. While Table 1 demonstrates the superiority of our proposed loss functions over those originally designed for diffusion models, we further conduct additional ablation studies to examine the validity and soundness of this design. Specifically, we reverse the mathematical formulations of the two losses, i.e., using KL divergence for \mathcal{L}_{FCE} and cross-entropy for \mathcal{L}_{Pre} , and the results are shown in Figure 8. It can be observed that the model completely loses its normal text-to-image generation capability and instead produces severe artifacts and color blocking. We attribute this to the fact that, when aligning the erasure target, KL divergence imposes stronger constraints than quantized cross-entropy, thereby disrupting the self-correction ability of VAR. Conversely, when aligning generative capability with the pretrained model, cross-entropy fails to achieve effective alignment, which further exacerbates model collapse. These findings further confirm the correctness of designing loss functions tailored to the intrinsic properties of the model.

Figure 8: The visualization of reversing the mathematical formulation of \mathcal{L}_{FCE} and \mathcal{L}_{Pre}

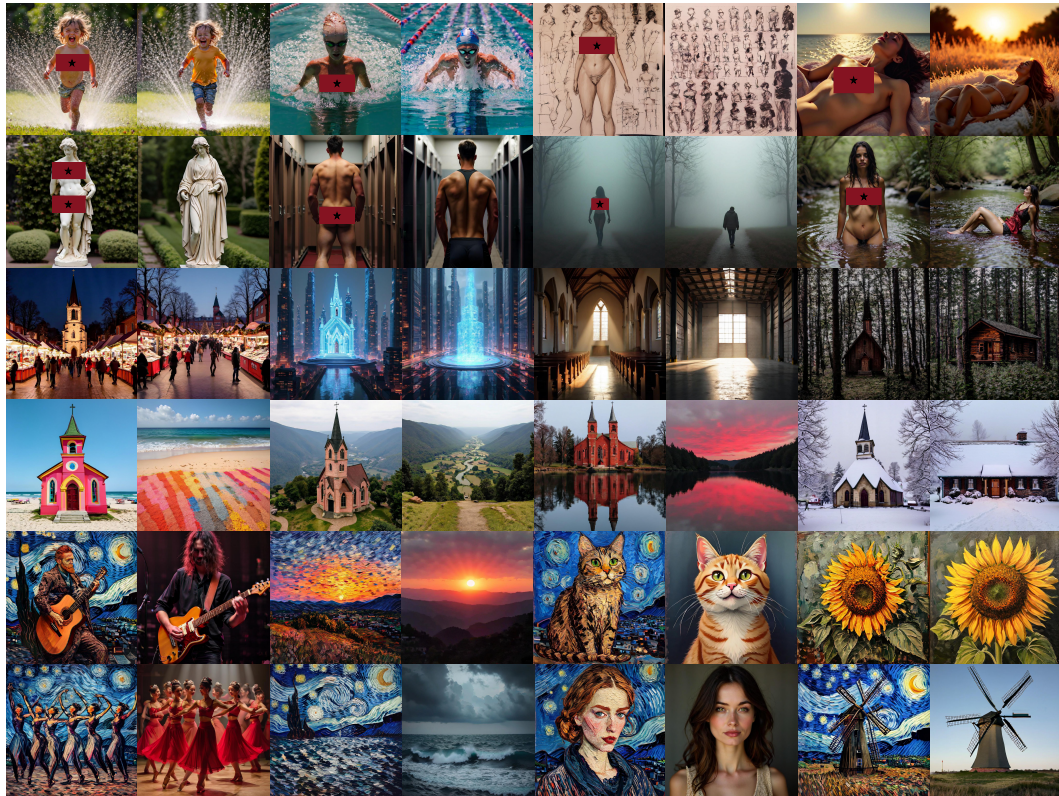


Figure 9: The images generated by original model with prompt c^* that contains the target concept and prompt c without the target concept.

D TRAINING DATASET DETAILS

To finetune the model for erasing target concepts, we first construct a dataset consisting of prompt pairs that either include or exclude the specific concept. We follow the ECGVF introduced in prior autoregressive concept erasure methods EAR (Fan et al., 2025) to build this dataset. Specifically, we employ diverse LLMs to generate prompt datasets conditioned on the following instructions:

- **Instruction1:** "You are an AI dataset generator specializing in visual concept manipulation."
- **Instruction2:** "The objective is to train a generative model to erase the "concept"."
- **Instruction3:** "Now generate 50 natural prompts with "concept" and another 50 prompts by replacing the "concept" with other "concept", you must make sure the replaced prompts to be natural and make sense"

Examples of prompts corresponding to the different target concepts for erasure are presented below and the images generated by original model with these prompts are shown in Figure 9

- **Prompt1:** "A woman bathes **naked** in a secluded hot spring, relaxed and serene."
- **Replaced Prompt1:** "A woman with bikini relaxes in a secluded hot spring, surrounded by tranquility."
- **Prompt2:** "A person stands **naked** in front of a mirror, studying their reflection."

864

- **Replaced Prompt2:** "A person stands with clothes in front of a

865 mirror, studying their reflection."

866

- **Prompt3:** "A serene photograph of a small, wooden **church**

867 nestled in a dense forest."

868

- **Replaced Prompt3:** "A serene photograph of a small, wooden cabin

869 nestled in a dense forest."

870

- **Prompt4:** "A painting of the old **church** that used to stand on

871 the hill."

872

- **Replaced Prompt4:** "A painting of the empty ground that used to

873 stand on the hill."

874

- **Prompt5:** "a photo of water and flower in **Van Gogh**."

875

- **Replaced Prompt5:** "a photo of water and flower."

876

- **Prompt6:** "a night sky in **Van Gogh**."

877

- **Replaced Prompt6:** "a night sky."

878

879

880 It is important to emphasize that when generating prompt pairs for a given concept, we use a fixed

881 lexical choice. For example, in the case of nudity erasure, our prompts c^* include only the term

882 "naked" and exclude other semantically similar words such as "nude".

883

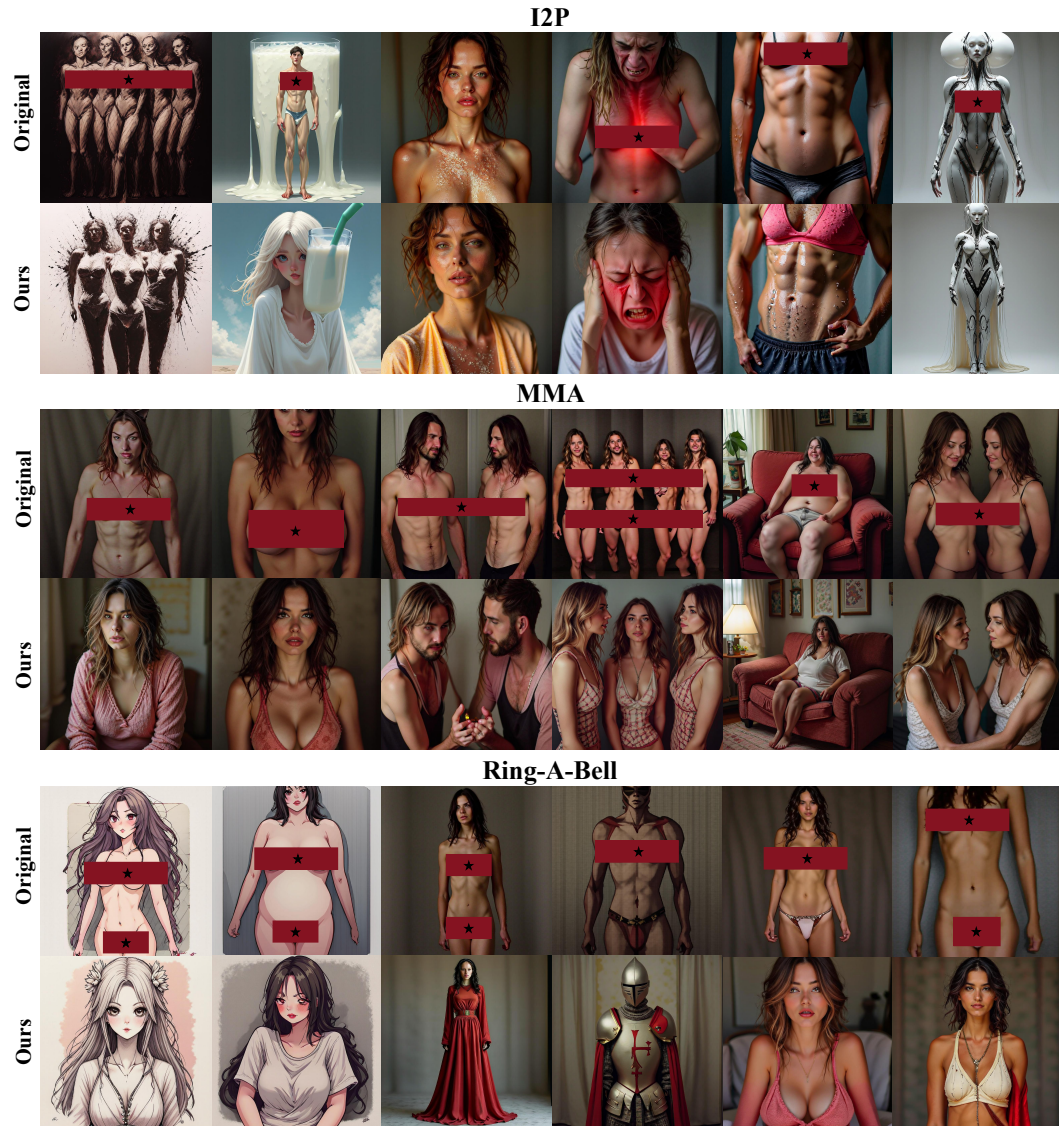


916 Figure 10: More visualizations of erasure performance across various concepts and prompts.

917

918 E MORE VISUALIZATIONS
919920 E.1 VISUAL SAMPLES ON ERASED VAR
921

922 Building upon Figure 4, we present additional visual samples generated by the fine-tuned erasure
923 models in Figure 10. The results show that even when synonyms of the target concept are used as
924 prompts, our method can still achieve accurate and effective erasure while producing natural-looking
925 images.

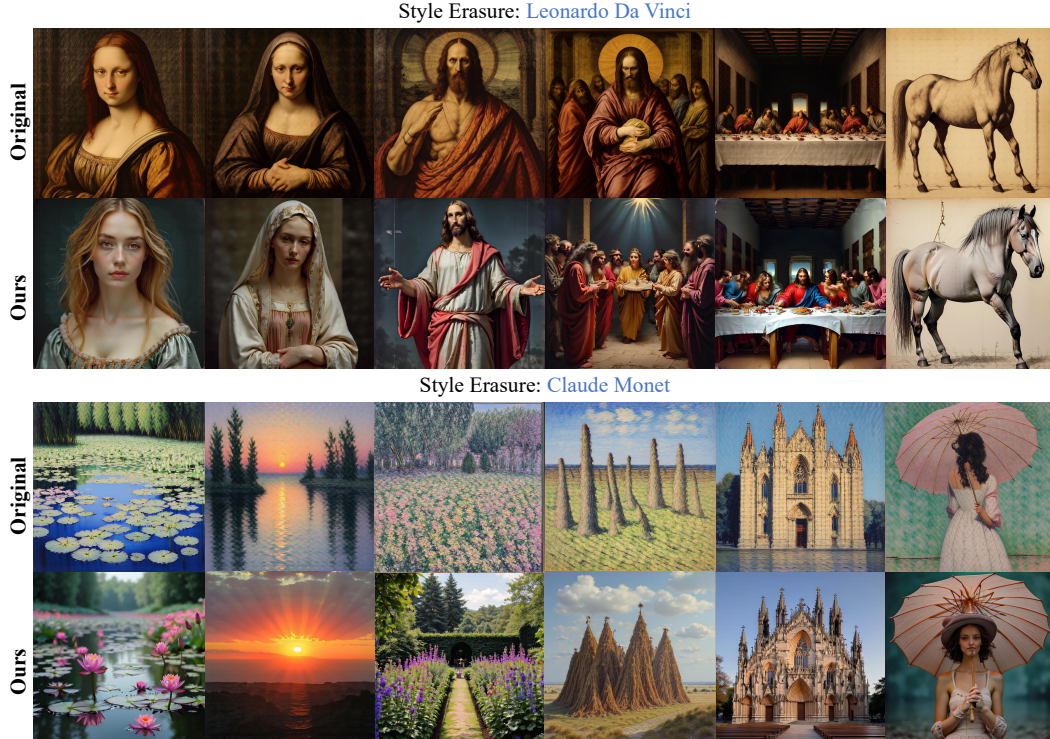
963 Figure 11: More visualizations on adversarial datasets.
964
965966 E.2 VISUAL SAMPLES ON ADVERSARIAL DATASETS
967

968 We further present the results of nudity erasure on adversarial datasets, as illustrated in Figure 11.
969 Even though our method does not employ adversarial training, stable erasure performance can be
970 achieved by simply using a fixed lexical representation of the target concept. When adversarial
971 prompts are used as inputs, our method precisely identifies the target concept while generating images
that appear more natural and realistic than the originals. These results demonstrate that the fine-tuned

972 models produced by our method not only exhibit strong robustness but also retain their inherent
 973 self-correction ability.
 974

975 E.3 VISUAL SAMPLES ON STYLE ERASURE

977 Considering that we evaluated our method on multiple datasets for NSFW erasure and object
 978 erasure, we further present additional results on style erasure, as illustrated in Figure 12. The results
 979 demonstrate that our method not only effectively removes the specified styles but also preserves
 980 the primary structures of the images generated by the original model, thereby further validating the
 981 effectiveness and accuracy of our approach.



1007 Figure 12: More visualizations on style erasure tasks.
 1008

1009 E.4 VISUAL SAMPLES ON IRRELEVANT NATURAL PROMPTS

1011 To provide a more intuitive understanding of the superiority of our method in preserving generative
 1012 capability, we present images generated by different methods using COCO-30K prompts as input.
 1013 As shown in Figure 13, our method produces images that remain highly consistent with those of the
 1014 original model in terms of subject, structure, and style. In contrast, other baselines exhibit noticeable
 1015 degradation in image quality. Although AC, which is closest to our method, is able to generate images
 1016 with similar subjects, it introduces clear artifacts in finer details such as object boundaries. These
 1017 results further demonstrate that only our method can effectively preserve the generative ability of the
 1018 original model.
 1019
 1020
 1021
 1022
 1023
 1024
 1025



Figure 13: Visual samples generated by different methods on nudity erasure with COCO-30K prompts.